Cement & Concrete Composites 43 (2013) 69–77

Contents lists available at SciVerse ScienceDirect

Cement & Concrete Composites

journal homepage: www.elsevier.com/locate/cemconcomp

# Accelerated carbonation – A potential approach to sequester $CO_2$ in cement paste containing slag and reactive MgO

Liwu Mo [a,b], Daman K. Panesar [a,*]

[a] Department of Civil Engineering, University of Toronto, Toronto, Ontario M5S 1A4, Canada
[b] College of Materials Science and Engineering, Nanjing University of Technology, Nanjing, Jiangsu 210009, China

ARTICLE INFO

*Article history:*
Received 8 December 2011
Received in revised form 15 June 2013
Accepted 6 July 2013
Available online 20 July 2013

*Keywords:*
Carbonation
$CO_2$ uptake
Microhardness
Microstructure
Reactive MgO
Slag

ABSTRACT

The cement industry and concrete producers are under pressure to reduce the carbon footprint and energy demands of cement-based construction materials. This study investigates the $CO_2$ uptake of paste mixtures designed with general use (GU) Portland cement, ground granulated blast furnace slag (GGBFS) and reactive MgO as cement replacement due to exposure to an accelerated carbonation curing regime with 99.9% concentration of $CO_2$. The $CO_2$ uptake, carbonation mechanism, microstructure and microhardness of cement pastes are examined. Key outcomes revealed that: (i) samples exposed to accelerated carbonation curing exhibit a denser microstructure and higher microhardness in comparison to non-carbonated samples, (ii) irrespective of the presence of reactive MgO, $CO_2$ uptake increases with age from 7 to 56 d, (iii) by 56 d, pastes containing 10% and 20% reactive MgO uptake similar amounts of $CO_2$ in comparison to mixtures without reactive MgO, and (iv) pastes containing 40% reactive MgO uptake the least amount of $CO_2$ however, exhibit the greatest microhardness and the lowest porosity.



## 1. Introduction

Concrete is the most widely used building material in the world. However, the current process for manufacturing cement is extremely energy intensive, and is also a significant contributor to $CO_2$ emissions, approximately 5% of global, anthropogenic $CO_2$ emissions [1]. Owing to the increasing awareness regarding sustainability, the cement industry is seeking ways to reduce its $CO_2$ emissions, decrease raw material inputs and lower the energy intensiveness of its processes. For decades, waste materials such as fly ash, blast furnace slag and silica fume have been used as supplementary cementing materials to replace conventional Portland cement [2–4]. Use of supplementary cementing materials improves concrete durability, and has economic and environmental benefits. However, despite these advantages, the cement industry and concrete producers remain under pressure to reduce both, greenhouse gas emissions and energy use and so have implemented initiatives in four primary areas: (i) reduction of energy required to manufacture cementing materials, (ii) alternative fuel sources, (iii) clinker substitution, and (iv) carbon capture and storage [5].

Mineral $CO_2$ sequestration, combining the alkaline earth metals (i.e. Ca, Mg) in Ca/Mg silica minerals such as olivine and serpentine with $CO_2$ to form stable Ca/Mg-bearing carbonate, is a safe and rapid approach for reducing industrial $CO_2$ emissions [6]. Prior to exposure to accelerated carbonation at elevated temperatures and/or pressures, minerals are chemically treated for instance acid extraction of Mg or Ca, or mechanically treated by grinding in order to increase the specific surface area [6–8]. Recognizing that these processes are costly and energy intensive [6,9], an alternative approach utilizes industrial solid alkaline wastes rich in Ca and/or Mg (i.e. steel slag, coal fly ash, cement kiln dust) as feedstock for the sequestration of $CO_2$ [10–14]. Cement-based materials exposed to air sequester $CO_2$ over their lifetime through carbonation processes [15–17]. Carbonation of cementitious materials is a diffusion controlled physicochemical process. The primary carbonation reaction that occurs between $CO_2$ and hydration products of conventional Portland cement is expressed as: $CO_2$ $(g \rightarrow aq) + Ca(OH)_2$ $(s \rightarrow aq) \rightarrow CaCO_3$ $(aq \rightarrow s) + H_2O$. Under natural conditions, carbonation can be a relatively slow process for concrete with low capillary porosity, but it can still yield detrimental long term effects related to reinforcing steel corrosion. On the other hand, researchers have begun to quantify the $CO_2$ uptake as a result of carbonation reactions to examine its role in partially off-setting greenhouse gas emissions associated with the cement manufacturing process [15–18]. Literature reports reveal that 7.6–57% of $CO_2$ produced during manufacture (the calcination process) of conventional cement could be reabsorbed by carbonation

* Corresponding author. Address: Department of Civil Engineering, University of Toronto, 35 St. George Street, Toronto, Ontario M5S 1A4, Canada. Tel.: +1 416 946 5712; fax: +1 416 978 6813.
*E-mail address:* d.panesar@utoronto.ca (D.K. Panesar).

0958-9465/$ - see front matter © 2013 Elsevier Ltd. All rights reserved.
http://dx.doi.org/10.1016/j.cemconcomp.2013.07.001

through the life-cycle of concrete [19,20]. Recognizing that the range of reported $CO_2$ uptake values is broad, and that for good quality concrete the rate natural carbonation is relatively slow, it is deduced that natural carbonation processes are an inefficient approach to mitigate global warming. Consequently, this study explores accelerated carbonation curing of cement-based materials and examines its implications on $CO_2$ uptake, cement chemistry and the hardened material properties [18,21]. In addition, exploring approaches to reduce the carbon footprint of cement and concrete by examining cement replacement alternatives is studied.

Reactive MgO as cement replacement has been used in relatively new cement-based materials such as 'Tech-Eco' and 'NovaCem' which have gained attention largely owing to their potential for $CO_2$ absorption [22,23]. 'Tech-Eco' contains reactive MgO produced by calcining magnesite ($MgCO_3$) at markedly lower temperatures (i.e. <750 °C) than the sintering temperature (up to 1450 °C) of cement clinker [22]. The reactive MgO in 'NovaCem' is extracted from magnesium silicates whereby it is reported that the process does not emit $CO_2$ [23]. To explore the $CO_2$ absorption potential of cement-based materials containing reactive MgO, some studies have exposed the reactive MgO cements to accelerated carbonation curing regimes using 5–20% $CO_2$ concentration [24]. Samples containing reactive MgO as cement replacement exposed to accelerated carbonation resulted in relatively stronger mechanical properties and a finer microstructure as a result of the formation of magnesium carbonates, including nesquehonite ($MgCO_3{\cdot}3H_2O$), dypingite ($Mg_5(CO_3)_4(OH)_2{\cdot}5H_2O$) and arinite ($Mg_2(OH)_2CO_3{\cdot}3H_2O$) [24,25].

This research investigates the ability of paste samples consisting of general use (GU) Portland cement, ground granulated blast furnace slag (GGBFS) and reactive MgO as cement replacement to sequester $CO_2$ by exposure to an accelerated carbonation curing regime. In this study the accelerated carbonation curing chamber is conditioned to 99.9% concentration $CO_2$, a 98% relative humidity, and a temperature of 23 ± 2 °C. The influence of GGBFS and reactive MgO as cement replacement on the carbonation mechanism, and the corresponding evolution of microstructure and microhardness is examined. This research is warranted given that fundamental quantitative analysis of the $CO_2$ uptake and the carbonation mechanism of cement blends containing GGBFS and reactive MgO as cement replacement have not been reported in the literature. Furthermore, this research is aligned with and compliments current efforts by the cement industry and concrete producers to reduce energy consumption, and $CO_2$ emissions.

## 2. Experimental

### 2.1. Materials, sample preparation and curing

The GU Portland cement and GGBFS used in this study were supplied by Holcim Canada. The reactive MgO was supplied by Liyang Special Materials Company, China. The reactive MgO mainly consists of magnesia, and a small amount of undecomposed $MgCO_3$ also exists. The reactive MgO powder has a maximum particle size of 80 μm, and a specific surface area of 54.6 $m^2/g$. Table 1 presents the chemical compositions of the GU cement, GGBFS, and reactive MgO.

Four paste mix designs were examined in this study all of which contain 40% GGBFS as cement replacement and have a water-to-binder ratio of 0.5. The primary mix design variable is the percentage of reactive MgO as cement replacement. As shown in Table 2, mixtures designated as M-0, M-10, M-20, and M-40 contain 0%, 10%, 20%, and 40% reactive MgO as cement replacement, respectively. For each mix design, two 20 × 20 × 300 mm paste prisms were prepared. The prisms were cured for 24 ± 2 h in an environment of 23 ± 2 °C, and 98% relative humidity and were then demoulded.

Once demoulded, one set of paste prisms was exposed to an accelerated carbonation environment of 99.9% $CO_2$ concentration, 98% relative humidity, and a temperature of 23 ± 2 °C until tested at 7 d, 28 d, and 56 d. The carbonation chamber condition is based on literature reports which emphasize the necessity of a high relative humidity for the formation of Mg-based carbonates such as nesquehonite ($MgCO_3{\cdot}3H_2O$) [24,25]. A 98% relative humidity was achieved with saturated $K_2SO_4$ solution [26]. The $CO_2$ pressure in the chambers was equal to atmospheric pressure. Prior to placing the specimens in the accelerated carbonation chamber, the prisms were vacuumed to 100 kPa below atmospheric pressure for 24 h in a desiccator with silica gel desiccant in order to facilitate the carbonation process by removal of excess moisture [27]. For comparison, the second set of paste prisms was cured in non-carbonated conditions consisting of natural $CO_2$ concentration (approximately 0.038%), 98% relative humidity, and a temperature of 23 ± 2 °C until tested at 7 d, 28 d, 56 d. The set of specimens stored in the 'non-carbonation environment' will be representative of and referred to as 'non-carbonated' specimens.

### 2.2. Test procedures

For each mix design, three 12–13 mm thick slices were sawn from the paste prisms after 7 d, 28 d, and 56 d of curing. The slices were dried in a desiccator with silica gel desiccant for 72 h by vacuuming to 100 kPa below atmospheric pressure. The specimens were then chemically and physically examined to: identify the formation of carbonation products, quantify the $CO_2$ uptake, characterize the microstructure, and measure the microhardness. Prior to conducting any tests on the carbonated specimens, the carbonation front was examined by spraying 1% phenolphthalein pH-indicator to the freshly-sawn paste surfaces.

#### 2.3.1. Identification of carbonate phases and quantification of $CO_2$ uptake

The dried paste slices were ground into a powder with a maximum particle size of 80 μm using a pestle and mortar. Crystalline phases present in the samples were analyzed by X-ray diffraction (XRD) analysis using an Analytical X-ray Powder Diffractometer with Cu Kα radiation ($\lambda$ = 1.5418 Å), 2$\theta$ range of 5–80°, and a step size of 0.02°. The $CO_2$ uptake in cement pastes was quantified by analyzing the mass loss due to decomposition of carbonate phases between 500 °C and 800 °C by Differential Thermal Analysis (DTA) and Thermogravimetric (TG) analysis using NETZSCH STA 409

**Table 1**
Chemical compositions of GU cement, GGBFS and reactive MgO (% by mass).

| | MgO | CaO | $SiO_2$ | $Al_2O_3$ | $Fe_2O_3$ | $Na_2O$ | $K_2O$ | $SO_3$ | LOI[a] |
|---|---|---|---|---|---|---|---|---|---|
| GU cement | 2.34 | 60.94 | 19.24 | 5.43 | 2.36 | 0.22 | 1.11 | 4.11 | 3.06 |
| GGBFS | 11.36 | 37.94 | 37.24 | 8.70 | 0.35 | 0.43 | 0.43 | 2.68 | 0.83 |
| MgO | 89.67 | 1.65 | 0.36 | 0.23 | 0.34 | 0.23 | 0.06 | – | 7.15 |

[a] LOI: Loss on ignition.

**Table 2**
Mix proportions of cement mixtures/weight %.

| | GU Portland cement | Reactive MgO | GGBFS |
|---|---|---|---|
| M-0 | 60 | 0 | 40 |
| M-10 | 50 | 10 | 40 |
| M-20 | 40 | 20 | 40 |
| M-40 | 20 | 40 | 40 |

instrument. During the DTA/TG analysis, the powder samples were heated from 25 °C to 1050 °C at a uniform rate of 10 °C/min with nitrogen gas flow of 50 ml/min.

*2.3.2. Pore structure analysis*

The pore size distribution and the total porosity of the specimens were characterized using a Quantachrome Autoscan 60 Mercury Intrusion Porosimeter (MIP). The apparent densities of samples were also determined from the MIP test.

*2.3.3. Image analysis*

A JEOL JSM6610-Lv Scanning Electron Microscope (SEM) coupled with an Oxford SDD (Silicon Drift Detector) Energy Dispersive X-ray (EDX) analysis detector was used for image and chemical analysis. The morphology of the carbonated phases was examined using SEM on the gold coated surface of the cement paste. For each mixture, one dried paste slice was epoxy resin impregnated, polished, carbon coated, and then its microstructure was investigated by Backscattered Scanning Electron Microscopy (BSEM).

*2.3.4. Microhardness test*

Sample microhardness was tested with a Vickers diamond pyramid indenter using a type 5100 Buehler Microhardness tester. A load of 0.981 N was applied on the polished surface of the samples with a dwell time of 10 s. A minimum of nine indentation tests were conducted on each sample.

## 3. Results and discussion

*3.1. Carbonation front*

For all four paste mixtures, no obvious color change was observed on the fresh fractured surfaces when sprayed with 1% phenolphthalein pH-indicator at 7 d, 28 d or 56 d. This indicates that the $CO_2$ penetrated throughout the cross section of the specimens after only 7 d of exposure to the accelerated carbonation environment.

*3.2. Carbonation products*

The XRD results shown in Fig. 1 reveals the formation of carbonation products for the four paste mixtures examined. The results indicate that at all ages, calcite and aragonite were the main carbonation products of paste mix M-0 and were also present in mixtures containing reactive MgO. Although aragonite was observed in all mixtures, the peak density decreased with increasing percentage of reactive MgO as cement replacement. Magnesian calcite and dolomite ($CaMg(CO_3)_2$) were also identified in pastes containing 10%, 20% and 40% reactive MgO. There were some weak peaks of magnesite which may be due to the undecomposed $MgCO_3$ present in the reactive MgO (raw material). Although the XRD patterns of magnesian calcite and calcite are similar making it difficult to discriminate between them, magnesian calcite was confirmed by SEM and EDX analysis which is detailed in Section 3.5. The XRD results shown in Fig. 1b and c indicate unique findings related to the M-40 mixture, specifically showing the formation of nesquehonite

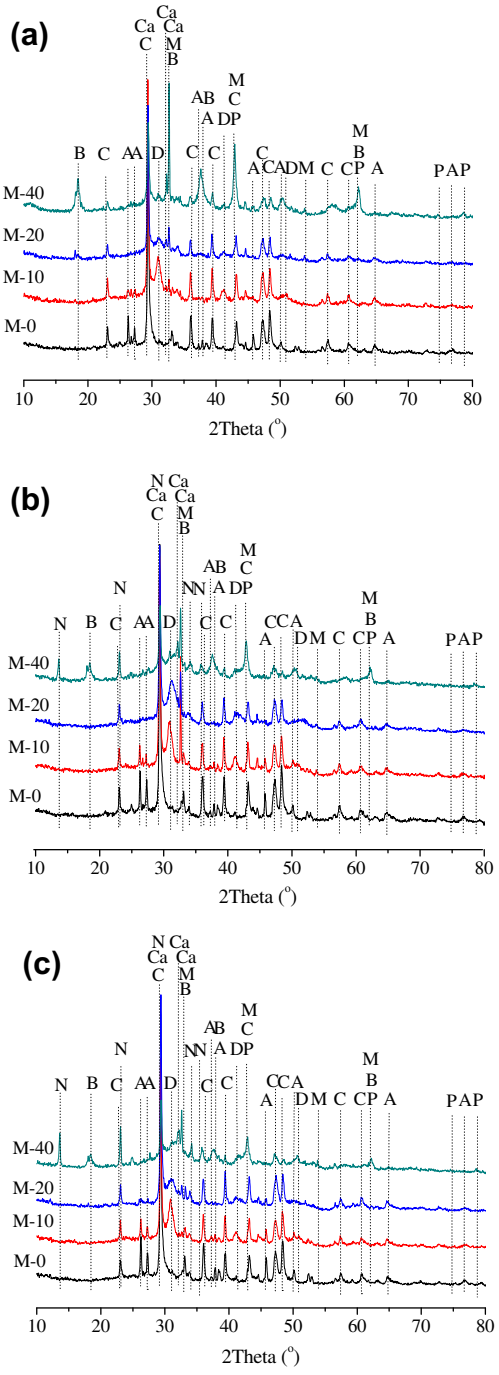


**Fig. 1.** XRD patterns of carbonated pastes, M-0, M-10, M-20, and M-40 at (a) 7 d, (b) 28 d and (c) 56 d (A: Aragonite, B: Brucite, C: Calcite (or Magnesia Calcite), Ca: Calcium Silicate, D: Dolomite, M: Magnesite, N: Nesquehonite, P: Magnesia).

($MgCO_3{\cdot}3H_2O$), and the presence of non-carbonated brucite ($Mg(OH)_2$) and MgO.

*3.3. $CO_2$ uptake*

The DTA/TG analysis of cement pastes after 56 d of exposure to the accelerated carbonation environment is shown in Fig. 2. For sample M-0, a clear decomposition peak is apparent at a temperature range of 750–900 °C in Fig. 2a, which is accompanied by a relatively large mass loss in Fig. 2b, due to the decomposition of calcite. For M-0 paste, Fig. 2b also shows a relatively significant

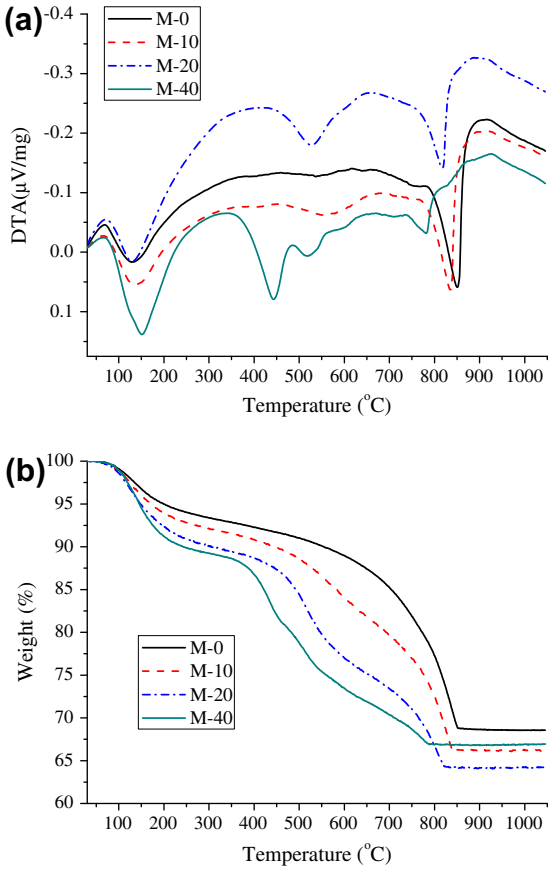


**Fig. 2.** Carbonated pastes after 56 d (a) DTA curves and (b) TG curves.

mass loss between 500 °C and 750 °C however, no corresponding endothermic peak is apparent in Fig. 2a. This may be associated with the decarbonation of amorphous calcium carbonates or aragonite [28]. Increasing the addition of reactive MgO from 0% to 40% as cement replacement yields a decrease in the peak temperature of decomposition from 850 °C to 780 °C as shown in Fig. 2a. This may be attributed to the formation of magnesian calcite by incorporating Mg in the $CaCO_3$ crystal. Furthermore, Fig. 2a shows the presence of additional endothermic peaks between 500 °C and 700 °C for pastes containing reactive MgO. This may be related to the decomposition of Mg-bearing carbonates, i.e. $CaMg(CO_3)_2$ and $MgCO_3{\cdot}3H_2O$ [29,30]. An obvious decomposition peak of $Mg(OH)_2$ at approximately 450 °C is also present in the DTA curve for sample M-40 and is also supported by the XRD results shown in Fig. 1b and c.

It is challenging to identify the exact mass loss corresponding to each carbonate phase due to the presence of overlapping endothermic peaks. However, since the mass loss that occurs between 500 °C and 850 °C is mainly associated with the decarbonation of calcium and/or magnesium carbonates it is used as the basis to estimate the total $CO_2$ uptake as summarized in Table 3. The estimated total $CO_2$ uptake by samples M-0, M-10, M-20, and M-40 after 56 d of exposure to $CO_2$ are 30.3%, 33.7%, 31.3%, and 18.0% (by the mass of blended mixtures after ignition), respectively. For all mixtures a significant amount of the $CO_2$ uptake occurred within the first 7 d of exposure. Approximately 93.2%, 80.1%, 63.9%, and 65.0% of the total 56 d $CO_2$ uptake occurred at 7 d for M-0, M-10, M-20, and M-40, respectively. Most of the $CO_2$ was sequestered at early ages, particularly for the mixtures containing 0% or 10% reactive MgO. The proportion of $CO_2$ sequestered from 7 d to 56 d in pastes containing reactive MgO was relatively higher than that of sample M-0 which is associated with the formation of Mg-bearing carbonates.

### 3.4. Pore structure

The pore size distribution of carbonated and non-carbonated cement pastes after 56 d is shown in Fig. 3. The results show that the non-carbonated specimens exhibit higher pore volumes of pores with diameters less than 0.07 μm in comparison to the carbonated specimens, irrespective of the presence of reactive MgO. However, the pore size distribution of the non-carbonated M-0 paste at pore diameters greater than 0.4 μm is finer than that of the corresponding carbonated M-0 sample. This observation is expected to be attributed to the presence of the GGBFS as cement replacement. It is well reported in the literature that pastes containing GGBFS are vulnerable to carbonation reactions yielding an increase in capillary porosity which has been attributed to the formation of soluble metastable calcium carbonates [31,32]. However, the interplay between GGBFS and reactive MgO appears to somewhat offset the effect of carbonation on the pore structure at intermediate concentrations (10% and 20%) of reactive MgO. In other words, although carbonation of GGBFS may lead to a coarser pore size distribution, the carbonation of reactive MgO has the opposite effect. This is supported by the results in Fig. 3 which shows that M-10 and M-20 carbonated specimens have relatively lower pore size distributions in comparison to M-0 and M-40 samples. Furthermore, the results reveal that at relatively large pore diameters, 1 μm, both the carbonated and non-carbonated M-40 specimens have similar pore volumes which are greater in comparison to the other mixtures. Closer examination of this observation is discussed in Section 3.5.

Fig. 4 shows the total pore volume of carbonated and non-carbonated paste specimens at 7 d, 28 d, and 56 d. After only 7 d of exposure, the total pore volumes of all carbonated cement pastes were less than the corresponding non-carbonated cement pastes after 56 d. With age, all carbonated specimens containing reactive MgO experienced a reduction in total porosity. In contrast, the carbonated mixture M-0 experienced minimal change in total porosity with age. This is likely to be attributed to the effect of GGBFS. Mixtures containing GGBFS have been shown to be more vulnerable to carbonation reactions in comparison to conventional Portland cement pastes in conditions of 40–80% relative humidity which typically results in a coarser pore structure [31,32]. However, because the carbonation chamber in this study is set to a 98% relative humidity the progress of carbonation reactions may be very slow. This supports the porosity measurements shown in Fig. 4. By 56 d, the M-0 paste has the greatest porosity and increasing percentage of reactive MgO reduces the porosity. This indicates that the incorporation of reactive MgO facilitates the reduction of pore volume in accelerated carbonation environments as a result

**Table 3**
Estimated $CO_2$ uptake in carbonated cement pastes (by mass of mixtures after ignition at 1050 °C, weight %).

| | M-0 | | | M-10 | | | M-20 | | | M-40 | | |
|---|---|---|---|---|---|---|---|---|---|---|---|---|
| | 7 d | 28 d | 56 d | 7 d | 28 d | 56 d | 7 d | 28 d | 56 d | 7 d | 28 d | 56 d |
| Estimated $CO_2$ uptake | 30.0 | 30.3 | 32.2 | 27.0 | 32.6 | 33.7 | 20.0 | 31.2 | 31.3 | 11.7 | 17.6 | 18.0 |

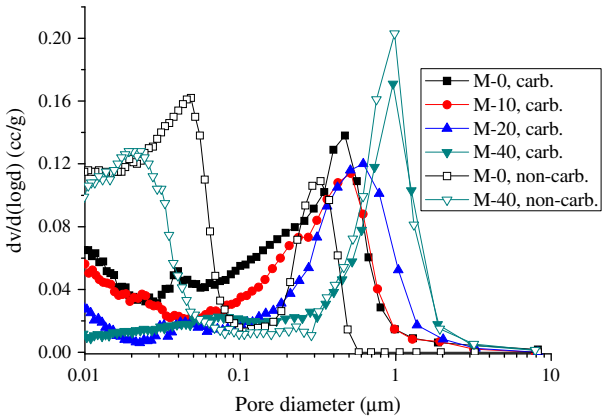


**Fig. 3.** Pore size distribution of non-carbonated and carbonated cement pastes after 56 d.

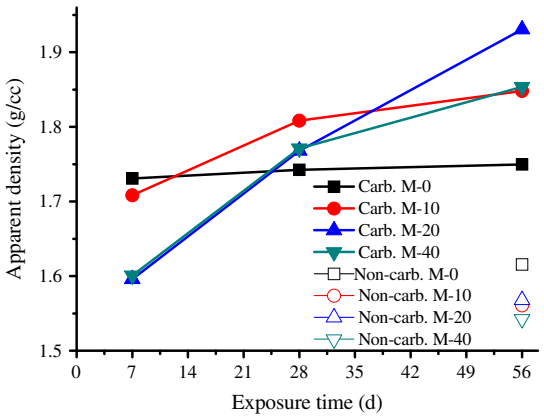


**Fig. 5.** Apparent densities of non-carbonated and carbonated cement pastes.

of the volume increase associated with the formation of Mg-based carbonated phases. Based on reported mineral densities [33], the transformation of $Ca(OH)_2$ to $CaCO_3$ can yield 11.4% increase of solid volume, while the transformation of MgO to $Mg(OH)_2$ and $MgCO_3{\cdot}3H_2O$, can yield approximately 131.4% and 614.3% increase in solid volume, respectively.

Fig. 5 shows that after only 7 d all of the carbonated pastes have greater apparent densities in comparison to the corresponding non-carbonated specimens after 56 d. The apparent density of cement pastes containing reactive MgO increases with age which is expected to be largely attributed to the formation of carbonates.

### 3.5. Microstructure

Fig. 6a shows a SEM image of sample M-0 after 56 d of accelerated carbonation exposure. The figure shows the formation of $CaCO_3$ agglomerates in and around the pores. The SEM images and EDX analysis of the carbonated samples M-20 and M-40 shown in Fig. 6b and c, respectively, reveals that the formation of intergrowth carbonates with round faces and edges manifest both in the pores and around the pore surfaces. The EDX elemental analysis shown in Fig. 6b and c identify the round carbonates as magnesian calcite as a result of incorporating Mg in $CaCO_3$ crystals during the precipitation process [34,35]. This validates the discussion of the XRD results presented in Fig. 1. In comparison to Fig. 6a of M-0 paste, Fig. 6c illustrates the presence of relatively greater amounts of magnesian calcite in carbonated M-40 paste. Furthermore, compared to the calcite formed in the M-0 specimen, the magnesian calcite in the M-40 samples is responsible for the dense connected microstructure due to its relatively larger crystal size and tighter conglomerate.

Fig. 7a, a BSEM image of carbonated M-0 sample after 56 d of accelerated carbonation curing, shows the precipitation of $CaCO_3$ as agglomerates in the pores, and the formation of dense carbonate layers on the pore surface. The GGBFS particle is surrounded by the carbonate layers (either calcite or magnesian calcite) which may obstruct the diffusion of $CO_2$ to the GGBFS particles and hinder its carbonation. Obvious non-carbonated hydration rims around the GGBFS grains are also visually apparent in Fig. 7a. Similar to M-0 specimens, the M-20 samples shown in Fig. 7b also illustrates the formation of carbonates in the pores, on the pore walls, and around the GGBFS particles. However, the carbonates in the M-20 samples consist mainly of magnesian calcite.

Fig. 8a shows that after 7 d of accelerated carbonation curing, the M-40 specimens contain considerable non-carbonated phases including GGBFS, $Mg(OH)_2$, and anhydrous cement clinker yielding a relatively porous structure, in comparison to later ages (i.e. 56 d) shown in Fig. 8b. After 56 d of exposure, $MgCO_3{\cdot}3H_2O$ was formed around the $Mg(OH)_2$, and the hydration rims around the GGBFS grains also carbonated, resulting in a relatively denser structure compared to that at 7 d.

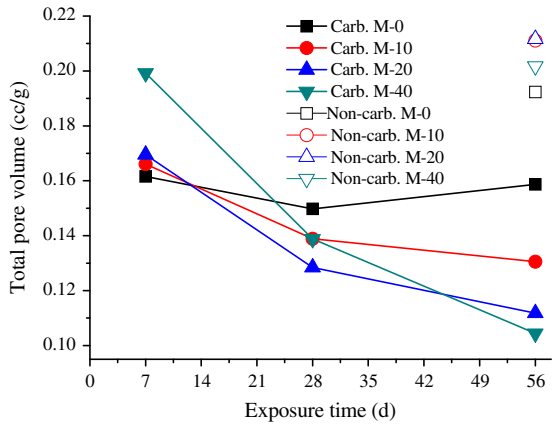


**Fig. 4.** Total pore volumes of non-carbonated and carbonated cement pastes.

### 3.6. Microhardness of cement pastes

The mean microhardness of non-carbonated and carbonated cement pastes containing various contents of reactive MgO is shown in Fig. 9. The data represents the average microhardness of nine measurements, and the corresponding coefficient of variation for the microhardness values ranged from 5% to 21%. The microhardness of the non-carbonated cement pastes increased with age, and achieved approximately 300 MPa at 56 d irrespective of addition of reactive MgO. For the carbonated pastes, the microhardness developed more rapidly owning to the formation of carbonates. After only 7 d of accelerated carbonation curing, the mean microhardness of all the pastes except M-40 was greater than of the non-carbonated pastes at 56 d. After 56 d of accelerated carbonation, the mean microhardness increased with increasing percentage of reactive MgO as cement replacement. For M-0, M-10, M-20, and M-40 the measured mean microhardness was 379, 416, 551, and 575 MPa, respectively. This result is closely associated with the influence of reactive MgO on the densification of the carbonated pastes and the carbonate morphology as discussed in Sections 3.4 and 3.5, respectively. The incorporation of Mg in $CaCO_3$ crystals influences the crystal morphology and enhances the inter-connection and agglomeration of carbonate crystals,

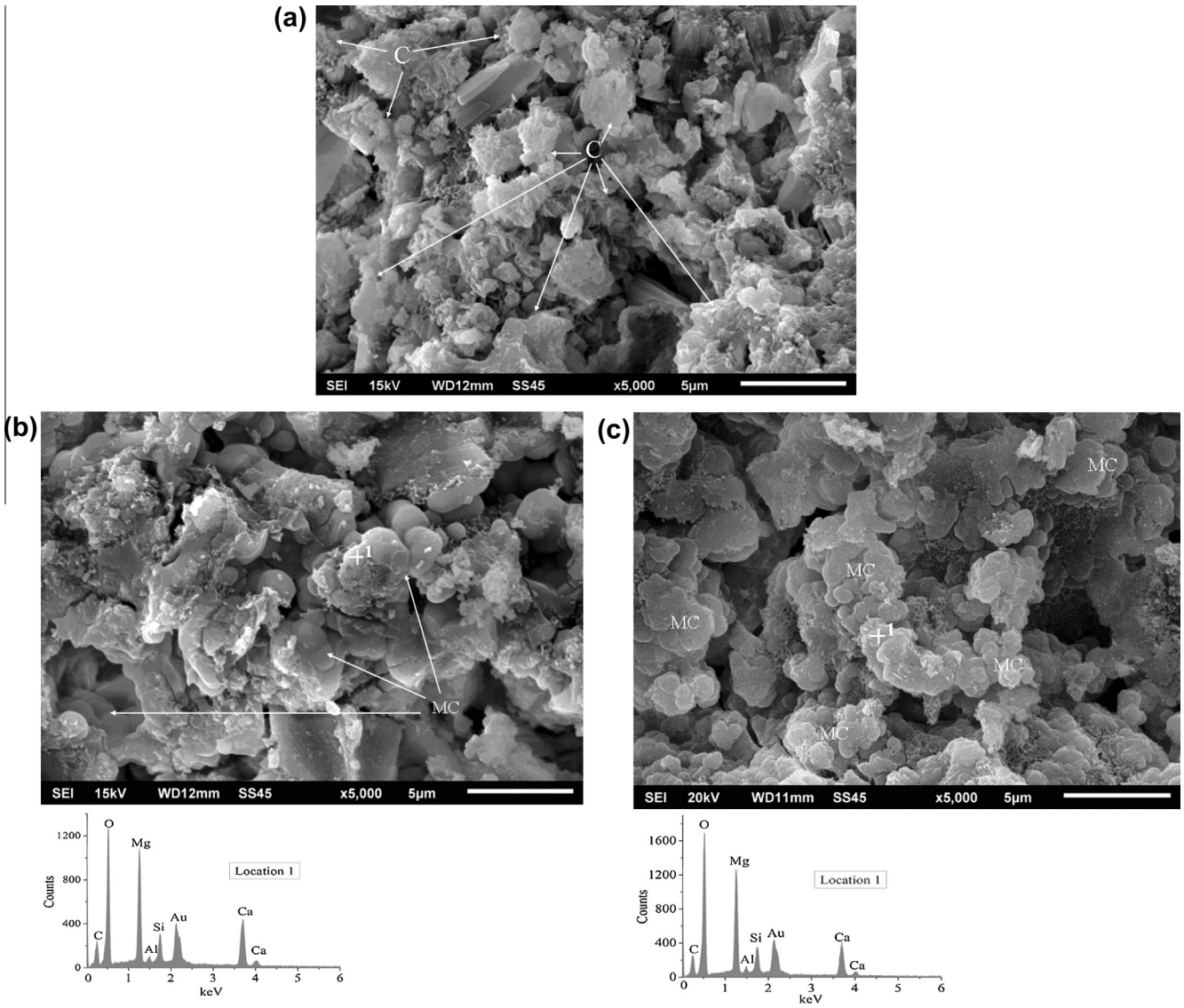


**Fig. 6.** SEM and EDX analysis of carbonated pastes after 56 d accelerated carbonation (a) M-0, (b) M-20 and (c) M-40 (C: Calcite, MC: Magnesian calcite).

which improves its mechanical performance. De Silva et al. [36] also found that the morphology of well-developed crystalline carbonates strongly influence the strength of carbonate binder.

### 3.7. Mechanism of $CO_2$ uptake

$CO_2$ sequestration of cement pastes containing 40% GGBFS as cement replacement and up to 40% reactive MgO as cement replacement occurs a result of chemical carbonation processes. After $CO_2$ diffused into the pore solution of cement pastes, and produces carbonate ions, it then reacts with $Ca^{2+}$ to precipitate $CaCO_3$. In M-0 specimens, $Ca^{2+}$ is available due to the dissolution of $Ca(OH)_2$, ettringite, and the decalcification of C–S–H (calcium silicate hydrate). The $Ca^{2+}$ ions may also be leached directly from anhydrous $C_2S$ (dicalcium silicate), $C_3S$ (tricalcium silicate) and GGBFS. Regardless of the different sources of $Ca^{2+}$, the precipitation process of $CaCO_3$ in the supersaturated solution is described as:

$$Ca^{2+}(aq) + CO_3^{2+}(aq) \rightarrow CaCO_3(s) \quad (1)$$

Figs. 6a and 7a illustrates the precipitation of $CaCO_3$ in the pore solution indicating that it is responsible for partially blocking capillary pores which may obstruct the diffusion of $CO_2$ from the external environment. At the same time, Fig. 7a shows that the $CaCO_3$ formed on the pore walls and on the surface of GGBFS particles is a dense carbonate layer which can bar the penetration of $CO_2$ from pores to potential carbonation sites namely, hydration products of cement and GGBFS.

For specimens M-10, M-20 and M-40, owing to the presence of $Mg^{2+}$ dissolved in the pore solution, the supersaturated solution contains both $Ca^{2+}$ and $Mg^{2+}$. Some of the $Mg^{2+}$ is incorporated into the $CaCO_3$ crystals to form magnesian calcite as shown in Fig. 6b and c and is described as:

$$Ca^{2+}(aq) + Mg^{2+}(aq) + CO_3^{2-}(aq) \rightarrow Ca_xMg_{1-x}CO_3(s) \quad (2)$$

Various Ca- and Mg-bearing carbonates such as low- and high-magnesian calcite, and even the $CaMg(CO_3)_2$, may be formed depending on the abundance of $Mg^{2+}$ indicated by the saturation index of $MgCO_3$ in solution [35]. Increasing $Mg^{2+}$ concentration in solution increases the Mg content in calcite crystals [37]. In $Mg^{2+}$-rich environments as in the case of the M-40 paste mixtures, magnesium carbonates such as $MgCO_3{\cdot}3H_2O$ may be formed [34,35] by the reaction described in Eq. (3):

$$Mg^{2+}(aq) + CO_3^{2-}(aq) + H_2O(aq) \rightarrow MgCO_3 \cdot 3H_2O(s) \quad (3)$$

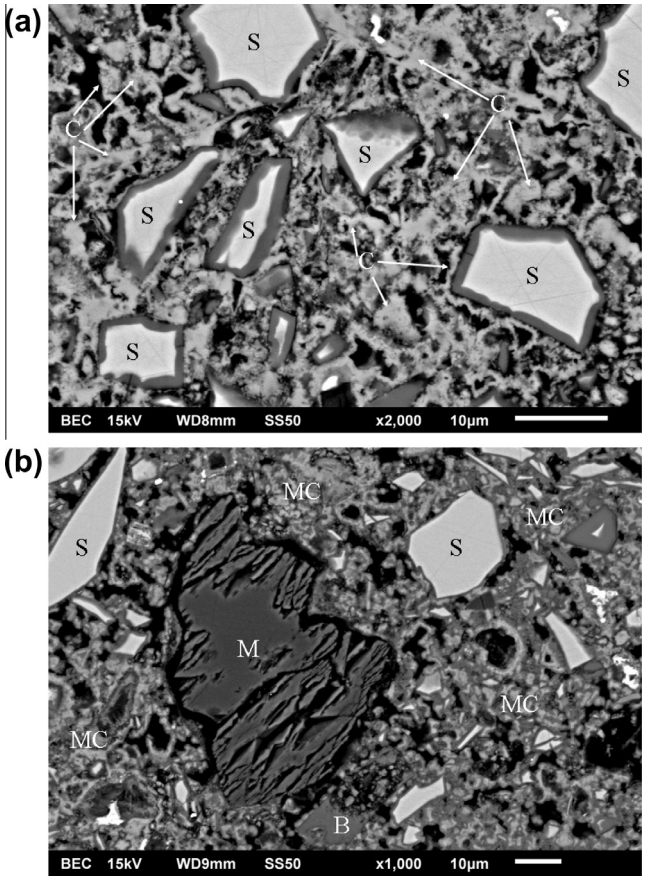


**Fig. 7.** BSEM images of carbonated pastes after 56 d of accelerated carbonation: (a) M-0 and (b) M-20. (B: Brucite, C: Calcite, MC: Magnesian calcite, S: GGBFS).

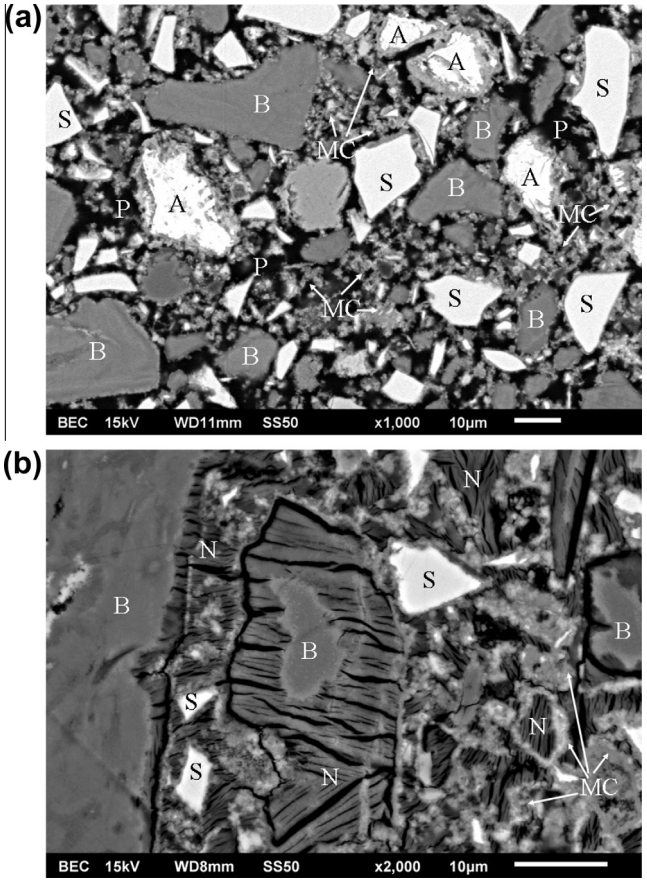


**Fig. 8.** BSEM image of carbonated M-40 pastes (a) 7 d, and (b) 56 d (A: Anhydrous cement clinker, B: Brucite, C: Calcite, M: Magnesite, MC: Magnesian calcite, N: Nesquehonite, S: GGBFS, P: Pores).

In this study, $MgCO_3{\cdot}3H_2O$ was formed in specimens containing 40% reactive MgO after 28 d and 56 d of carbonation.

The rate and capacity of $CO_2$ sequester in the cement pastes containing GGBFS and reactive MgO as cement replacement is dependent on two main factors. Firstly, the dissolving rate, content, and diffusion of $Ca^{2+}$ and $Mg^{2+}$ from the Portland cement, GGBFS, and reactive MgO into the pore solution, and secondly, the rate of dissolving $CO_2$ in water and its transport through the paste's capillary pore network. Regarding the former, cement hydration product, $Ca(OH)_2$, dissolves relatively easily in the pore solution, and so carbonates quickly. After only 7 d of exposure, all the $Ca(OH)_2$ is carbonated, as supported by the XRD results in Fig. 1. With depletion of $Ca^{2+}$, $Ca^{2+}$ may be released from the decomposition of ettringite, and C–S–H [18]. As a result of diffusion of $Ca^{2+}$ and $CO_3^{2-}$, Ca-bearing carbonates form a carbonate layer on the surfaces of MgO and GGBFS particles.

Leaching of $Ca^{2+}$ from GGBFS may be the rate-determining reaction step for GGBFS carbonation [11]. The amount of $Ca^{2+}$ and $Mg^{2+}$ leached directly from GGBFS particles may be limited due to the barrier of hydration product rim and carbonate layers formed around the GGBFS particle as shown in Fig. 7 and 8. Reactive MgO is easily transformed into $Mg(OH)_2$ due to hydration, and then carbonated. Since the solubility of $Mg(OH)_2$ is only approximately 1/200 of that of $Ca(OH)_2$ [38], a relatively small amount of $Mg^{2+}$ dissolves in the pore solution, limiting the carbonation rate of $Mg(OH)_2$. Moreover, the low solubility of $Mg(OH)_2$ and the physical barrier of the Ca-bearing carbonate layer are expected to reduce the rate of $Mg^{2+}$ diffusion. However, the $CO_3^{2-}$ and/or $Ca^{2+}$ ions can diffuse through the carbonate layer into the $Mg^{2+}$-rich region around the $Mg(OH)_2$, and locally form high-magnesian calcite, and even $MgCO_3{\cdot}3H_2O$ as shown in Figs. 7b and 8b.

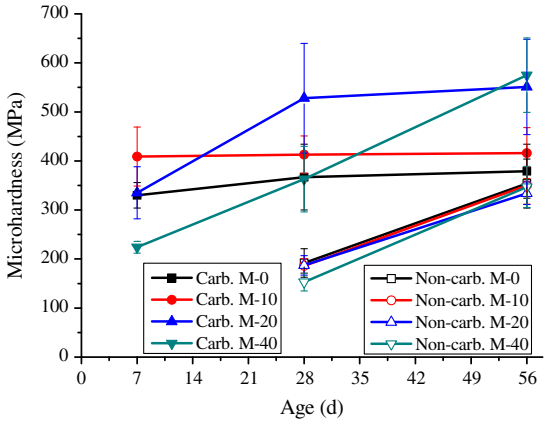


**Fig. 9.** Microhardness of non-carbonated and carbonated cement pastes.

## 4. Conclusions

The $CO_2$ uptake capacity, carbonation mechanism, microstructure evolution, and microhardness of blended cement pastes containing 40% GGBFS and 0–40% reactive MgO during curing in an accelerated carbonation environment was investigated. Outcomes from this study reveal that the utilization of intermediate percentages of reactive MgO, up to 20% cement replacement, exhibits similar $CO_2$ uptake as compared to mixtures with 0% and 10% reactive MgO as early as 28 d, and enhances the quality of the paste's

microstructure or microhardness. The carbonation mechanism and examination of its implications on the paste's hardened properties is complex. Key conclusions regarding the chemistry and morphology of Ca and Mg bearing carbonate phases with age and the effect on microstructure and microhardness are described below.

(1) Under the accelerated carbonation condition of 99.9% concentration $CO_2$, all the blended cement pastes irrespective of the presence of reactive MgO carbonated rapidly with most of the $CO_2$ uptake occurring with the first 7 d. Approximately 11.7–30.0% $CO_2$ by mass of raw mixes after ignition was sequestered after 7 d due to the formation of calcium and/or magnesium carbonates. From 7 to 56 d, carbonation reactions continued more for mixtures containing reactive MgO than mixtures without reactive MgO (M-0). By 56 d, cement pastes containing 10 and 20% reactive MgO uptake similar amounts of $CO_2$ in comparison to mixtures without reactive MgO. Cement pastes containing 40% reactive MgO uptake the least amount of $CO_2$, implying the reactive MgO does not improve the $CO_2$ uptake.
(2) Calcite and aragonite were the main calcium carbonates formed in the pastes without reactive MgO as cement replacement. For mixtures containing 10%, 20%, and 40% reactive MgO, the Mg-bearing carbonate phases formed were magnesian calcite and $CaMg(CO_3)_2$. In addition, $MgCO_3{\cdot}3H_2O$ was formed in the blended cement paste containing 40% reactive MgO.
(3) Ca/Mg carbonates, namely, calcite, and magnesian calcite precipitated as agglomerates in pores and as dense carbonate layer around the pore wall, $Mg(OH)_2$, and GGBFS particles, limiting the penetration of $CO_2$ and diffusion of ions such as $Ca^{2+}$, $Mg^{2+}$, and $CO_3^{2-}$. Due to the low solubility of $Mg(OH)_2$, and slow leaching of $Ca^{2+}$ from GGBFS, the carbonation rate of reactive MgO and GGBFS are relatively lower than that of Portland cement hydration product $Ca(OH)_2$.
(4) In comparison to the non-carbonated cement pastes, the formation of Ca/Mg carbonates reduced the pore size distribution and pore volume, and increased the microhardness. The incorporation of reactive MgO in cement pastes contributes to the tight morphology and conglomeration of carbonate phases, resulting in higher microhardness. The effects of reactive MgO on the strength of cement pastes are of interest, which will be investigated further in our forthcoming study.
(5) Additional research efforts aimed towards decoupling the effect of hydration and carbonation for ternary systems (GU, GGBFS and reactive MgO) and the size effect of specimens in accelerated carbonation environments is warranted.

## Acknowledgements

Valuable input to this study by Dr. O. Perebatova, Prof. K. Peterson, Prof. R.D. Hooton, Dr. D. Grozea, Mr. B. Tang, and Dr. G. Kretschmann from University of Toronto, Canada is appreciated. Prof. M. Deng and Mr. A. Lu from Nanjing University of Technology, China are acknowledged for providing reactive MgO powders. Financial support from the National Science and Engineering Research Council of Canada, China Scholarship Council/The University of Toronto Joint Scholarship, and continued support by way of the ERA from the Ministry of Economic Development and Innovation is acknowledged. In addition, Jiangsu Natural Science Fund (BK2012427), and the research fund of Key Laboratory for Advanced Technology in Environmental Protection of Jiangsu Province (AE201105) are also gratefully acknowledged.

## References

[1] Cement Technology Roadmap 2009, Carbon emissions reductions up to 2050. International Energy Agency and World Business Council for Sustainable Development <http://www.wbcsd.org/DocRoot/mka1EKor6mqLVb9w903o/WBCSD-IEA_CementRoadmap.pdf> (date accessed 09.13.11).
[2] Al-Amoudi OSB, Maslehuddin M, Ibrahim M, Shameem M, Al-Mehthel MH. Performance of blended cement concretes prepared with constant workability. Cem Concr Compos 2011;33(1):90–102.
[3] Malhotra VM, Hemmings RT. Blended cements in North America – a review. Cem Concr Compos 1995;17(1):23–35.
[4] Lothenbach B, Scrivener K, Hooton RD. Supplementary cementitious materials. Cem Concr Res 2011;41(3):217–29.
[5] Schneider M, Romer M, Tschudin M, Bolio H. Sustainable cement production-present and future. Cem Concr Res 2011;41(7):642–50.
[6] Huijgen WJJ, Comans RNJ. Carbon dioxide sequestration by mineral carbonation literature review update 2003–2004. Petten: Energy Research Centre of the Netherlands; 2005.
[7] Krevor SC, Lackner KS. Enhancing process kinetics for mineral carbon sequestration. Energy Procedia 2009;1:4867–71.
[8] Maroto-Valer MM, Fauth DJ, Kuchta ME, Zhang Y, Andresen JM. Activation of magnesium rich minerals as carbonation feedstock materials for $CO_2$ sequestration. Fuel Process Technol 2005;86:1627–45.
[9] Huijgen WJJ, Comans RNJ, Witkamp GJ. Cost evaluation of $CO_2$ sequestration by aqueous mineral carbonation. Energy Convers Manage 2007;48(7):1923–35.
[10] Huijgen WJJ, Comans RNJ. Carbonation of steel slag for $CO_2$ sequestration: leaching of products and reaction mechanisms. Environ Sci Technol 2006;40(8):2790–6.
[11] Huijgen WJJ, Witkamp GJ, Comans RNJ. Mineral $CO_2$ sequestration by steel slag carbonation. Environ Sci Technol 2005;39(24):9676–82.
[12] Montes-Hernandez G, Pérez-López R, Renard F, Nieto JM, Charlet L. Mineral sequestration of $CO_2$ by aqueous carbonation of coal combustion fly-ash. J Hazard Mater 2009;161:1347–54.
[13] Huntzinger DN, Gierke JS, Kawatra SK, Eisele TC, Sutter LL. Carbon dioxide sequestration cement kiln dust through mineral carbonation. Environ Sci Technol 2009;43(6):1986–92.
[14] Sipilä J, Teir S, Zevenhoven R. Carbon dioxide sequestration by mineral carbonation Literature review update 2005–2007. Turku: Åbo Akademi University; 2008.
[15] Panesar DK, Churchill CJ. The influence of design variables and environmental factors on life-cycle cost assessment of concrete culverts. Struct Infrastruct Eng V 2013;9(3):201–213.
[16] Lagerblad B. State of the art: $CO_2$ uptake during concrete life cycle. Stockholm: Swedish Cement and Concrete Research Institute; 2006.
[17] Pade C, Guimaraes M. The $CO_2$ uptake of concrete in a 100 year perspective. Cem Concr Res 2007;37(9):1348–56.
[18] Monkman S, Shao Y. Integration of carbon sequestration into curing process of precast concrete. Can J Civ Eng 2010;37(2):302–10.
[19] Galan I, Andrade C, Mora P, Sanjuan MA. Sequestration of $CO_2$ by concrete carbonation. Environ Sci Technol 2010;44(8):3181–6.
[20] Kjellsen KO, Guimaraes M, Nilsson Å. The $CO_2$ balance of concrete in a life cycle perspective. Taastrup: Danish Technological Institute; 2005.
[21] Shi C, Wu Y. $CO_2$ curing of concrete blocks. Concr Int 2009(February):39–43.
[22] T. Tececo Pty Ltd. Australia, US Patent 7347896; 2008.
[23] Novacem Limited. Novacem carbon negative cement: presentation for SCI, 25 November, 2010. <http://novacem.com/wp-content/uploads/2010/12/20101125-Technical-update.pdf>.
[24] Vandeperre LJ, Al-Tabbaa A. Accelerated carbonation of reactive MgO cements. Adv Cem Res 2007;19(2):67–79.
[25] Liska M, Al-Tabbaa A. Ultra-green construction: reactive magnesia masonry products. Proc Inst Civil Eng, Waste Resour Manage 2009;162(WR0):1–12.
[26] Young JF. Humidity control in the laboratory using salt solutions – a review. J Appl Chem 1967;17(9):241–5.
[27] Venhuis MA, Reardon EJ. Vacuum method for carbonation of cementitious wasteforms. Environ Sci Technol 2001;35(20):4120–5.
[28] Thiery M, Villain G, Dangla P, Platret G. Investigation of the carbonation front shape on cementitious materials: effects of the chemical kinetics. Cem Concr Res 2007;37(7):1047–58.
[29] Samtani M, Dollimore D, Alexander KS. Comparison of dolomite decomposition kinetics with related carbonates and the effect of procedural variables on its kinetic parameters. Thermochim Acta 2002;392–393:135–45.
[30] Lanas J, Alvarez JI. Dolomitic lime: thermal decomposition of nesquehonite. Thermochim Acta 2004;421(1–2):123–32.
[31] Stark J, Ludwig H-M. Freeze-deicing salt scaling resistance of concretes containing blast-furnace slag-cement. In: Marchand J, Pigeon M, Setzer M, editors. Freeze–thaw durability of concrete. E&FN Spon; 1997. p. 107–20.
[32] Tumidajski PJ, Chan GW. Boltzmann–Matano analysis of chloride diffusion in to blended cement concrete. J Mater Civ Eng 1996;8(4):195–200.
[33] Mineralogy Database. <http://webmineral.com.>
[34] De Silva P, Bucea L, Sirivivatnanon V. Chemical, microstructural and strength development of calcium and magnesium carbonate binders. Cem Concr Res 2009;39(5):460–5.

[35] Pokrovsky OS. Precipitation of calcium and magnesium carbonates from homogeneous supersaturated solutions. J Cryst Growth 1998;186(1):233–9.
[36] De Silva P, Bucea L, Moorehead DR, Sirivivatnanon V. Carbonates binders: reaction kinetics, strength and microstructure. Cem Concr Compos 2006;28(7):613–20.
[37] Meldrum FC, Hyde ST. Morphological influence of magnesium and organic additives on the precipitation of calcite. J Cryst Growth 2001;231(4):544–58.
[38] Engineering and Design – Precipitation/Coagulation/Flocculation Publication Number: EM 1110-1-4012. U.S. Army corps of Engineers: Washington, DC 20314-1000; 2001.